ACS APPLIED MATERIALS & INTERFACES

www.acsami.org

Research Article

Integrating Structural Colors with Additive Manufacturing Using Atomic Layer Deposition

Benjamin A. Rorem,[⊥] Tae H. Cho,[⊥] Nazanin Farjam, Julia D. Lenef, Kira Barton,* Neil P. Dasgupta,* and L. Jay Guo*

Cite This: *ACS Appl. Mater. Interfaces* 2022, 14, 31099–31108

Read Online

ACCESS | Metrics & More | Article Recommendations | Supporting Information

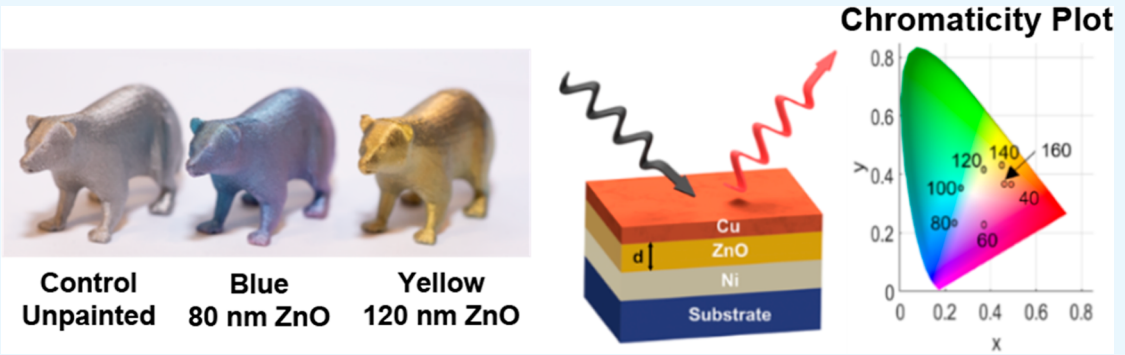

ABSTRACT: We demonstrate tunable structural color patterns that span the visible spectrum using atomic layer deposition (ALD). Asymmetric metal−dielectric−metal structures were sequentially deposited with nickel, zinc oxide, and a thin copper layer to form an optical cavity. The color response was precisely adjusted by tuning the zinc oxide (ZnO) thickness using ALD, which was consistent with model predictions. Owing to the conformal nature of ALD, this allows for uniform and tunable coloration of non-planar three-dimensional (3D) objects, as exemplified by adding color to 3D-printed parts produced by metal additive manufacturing. Proper choice of inorganic layered structures and materials allows the structural color to be stable at elevated temperatures, in contrast to traditional paints. To print multiple colors on a single sample, polymer inhibitors were patterned in a desired geometry using electrohydrodynamic jet (e-jet) printing, followed by area-selective ALD in the unpassivated regions. The ability to achieve 3D color printing, both at the micro- and macroscales, provides a new pathway to tune the optical and aesthetic properties during additive manufacturing.

KEYWORDS: *structural color, additive manufacturing, Fabry−Pérot, atomic layer deposition, electrohydrodynamic jet printing, area-selective deposition*

INTRODUCTION

Surfaces that exhibit structural color with tunable reflection spectra are desired in many applications, such as optical displays, prints, decorations, and colored photovoltaics.[1−13] Compared to pigment-based color, structural color offers many advantages including high brightness, durability, environmental sustainability, and ease of fabrication.[14] A simple geometry that produces vibrant color is a three-layer Fabry−Pérot cavity, which can be produced with vacuum deposition or electrodeposition techniques.[15−17] However, traditional thin-film deposition processes are often affected by tradeoffs between conformality, thickness control, and versatility in material selection. For example, physical vapor deposition (PVD) techniques are limited in their ability to deposit conformal films on complex three-dimensional (3D) structures with high aspect ratios, while electrodeposition is limited to electrically conductive materials.

To overcome these tradeoffs, atomic layer deposition (ALD) is a powerful vapor-phase deposition process that affords unparalleled control of film thickness and conformality, owing to the self-limiting nature of surface reactions.[18,19] The previous literature has shown that by tuning the processing conditions, ALD precursors can infiltrate through ultrafine pores to provide uniform coatings with ultra-high aspect ratios (>50,000:1)[20] and can conformally coat complex topologies with re-entrant texture, without gradients in film thickness or composition.[21−25] Furthermore, many ALD processes can be

Received: April 4, 2022
Accepted: June 16, 2022
Published: July 4, 2022

https://doi.org/10.1021/acsami.2c05940
ACS Appl. Mater. Interfaces 2022, 14, 31099−31108

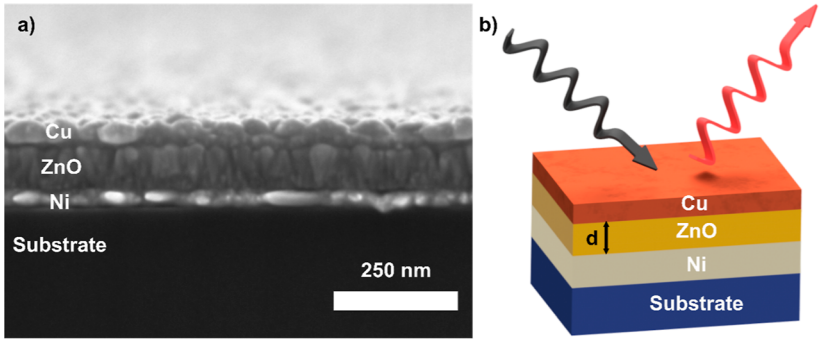

Figure 1. (a) Cross-sectional SEM image of deposited MDM structure with 50 nm thick Ni, 120 nm of ALD ZnO, and 20 nm of ALD Cu metal. (b) Schematic of MDM structure with incoming white light and outgoing colored light where ZnO thickness, *d*, can be tuned to determine the resonance of the light cavity.

performed at relatively low temperatures (typically <250 °C), which is compatible with a wide range of substrate materials including flexible polymers or biological/organic templates.[21,26,27] More recently, advances in spatial ALD processes and instrumentation have increased the throughput of ALD by several orders of magnitude and are compatible with roll-to-roll manufacturing.[28−30] These attributes of ALD make it an ideal method to integrate with additive manufacturing processes such as 3D printing as ALD films can conformally modify complex object surfaces with sub-nanometer precision in composition, thickness, and structure. However, the integration of ALD with additive manufacturing remains in its infancy.[31,32]

While the ability of ALD to uniformly coat the entire surface of 3D objects is desirable in many applications, in other instances, it is desirable to selectively deposit ALD films only in specific locations. This can be achieved through area-selective ALD (AS-ALD), which utilizes surface modifications to deactivate the ligand-exchange reactions between precursor molecules and surface functional groups.[33−43] We have recently demonstrated that AS-ALD can be achieved using polymer inhibitors deposited by electrohydrodynamic jet (e-jet) printing.[44,45] Ink-jet printing was used recently to make multicolor prints on the same sample,[46] but e-jet-based nano-/micro-additive manufacturing process is superior to ink-jet printing in terms of enabling (1) printing a broader range of materials such as viscous polymers, conductive nanoparticle suspensions, and biomaterials and (2) sub-micron resolution patterning in the $x-y$ plane, which is significantly higher resolution than ink-jet processes (typically >50 μm). The combination of e-jet printing with AS-ALD enables additive nanomanufacturing with sub-100 nm resolution in the $x-y$ plane and sub-nanometer resolution in the z-direction.[47−49] Moreover, while printing processes are often limited by available ink materials, ALD can be used to deposit a versatile range of functional materials with tunable electronic, optical, and mechanical properties, including metals, metal oxides, sulfides, nitrides, and polymers (using molecular layer deposition).[50]

In this study, we propose to leverage these attributes of ALD to solve an important challenge in the additive manufacturing field: how can we tunably modify the color of 3D-printed objects with complex (non-planar) topologies? Traditionally, the optical properties of additively manufactured parts are limited by the inks or powders used as source materials, which are restricted by their thermal, mechanical, and chemical properties. While some surfaces may be compatible with paints or dye chemicals, these processes are limited in their ability to conformally penetrate high-aspect-ratio geometries, require specific chemical compatibilities, and are susceptible to fading and/or delamination in ambient environments. Therefore, to decouple the "bulk" geometric properties of a printed object from its optical response, we propose the integration of structural color with additive manufacturing using ALD surface modifications.

Many structural colors have been fabricated with simple thin-film structures, such as pearlescent coatings and nanoscale dielectric layers on metal substrates.[51−53] However, these single-layered coatings typically have low-quality factor and poor color purity.[54] Alternatively, high color purity can be achieved with a three-layer cavity, consisting of a dielectric layer sandwiched between two metal layers [metal−dielectric−metal (MDM)]. The base metal layer acts as a visible broadband reflector, the dielectric layer determines the resonance of the light cavity, and the top metal layer acts as an absorber to increase the color vibrancy.[10] The top metal layer must be thinner than the optical skin depth so that light can penetrate into the dielectric layer. Certain wavelengths will destructively interfere upon reflection, depending on non-trivial reflection phase shifts due to lossy metals and the phase picked up during propagation through the dielectric. Therefore, by tuning the thickness of the dielectric layer coatings and thus adjusting the propagation phase, the structural coloration can be precisely manipulated.

In this work, we demonstrate the ability of ALD to produce MDM structures with a wide range of vibrant structural colors, which can be precisely tuned by controlling the dielectric layer thickness. We apply these coatings to rationally control the color of metal 3D-printed objects with complex, non-planar topologies. This yields a pigment-free method of "painting" 3D-printed objects with excellent conformality. An additional ALD dielectric layer not only protects the thin metal layer from oxidizing but also enhances the color saturation by improving the light absorption and reflection at appropriate wavelengths. We further demonstrate multi-color MDM patterns produced using AS-ALD patterned by e-jet printing, facilitating color printing of functional materials above the resolution limits of ink-jet. This approach can serve as a platform to integrate versatile color palettes onto 3D-printed objects with complex topologies spanning the nano- to macroscales, which opens new opportunities to apply additive manufacturing for applications where aesthetics are important.

https://doi.org/10.1021/acsami.2c05940
ACS Appl. Mater. Interfaces 2022, 14, 31099−31108

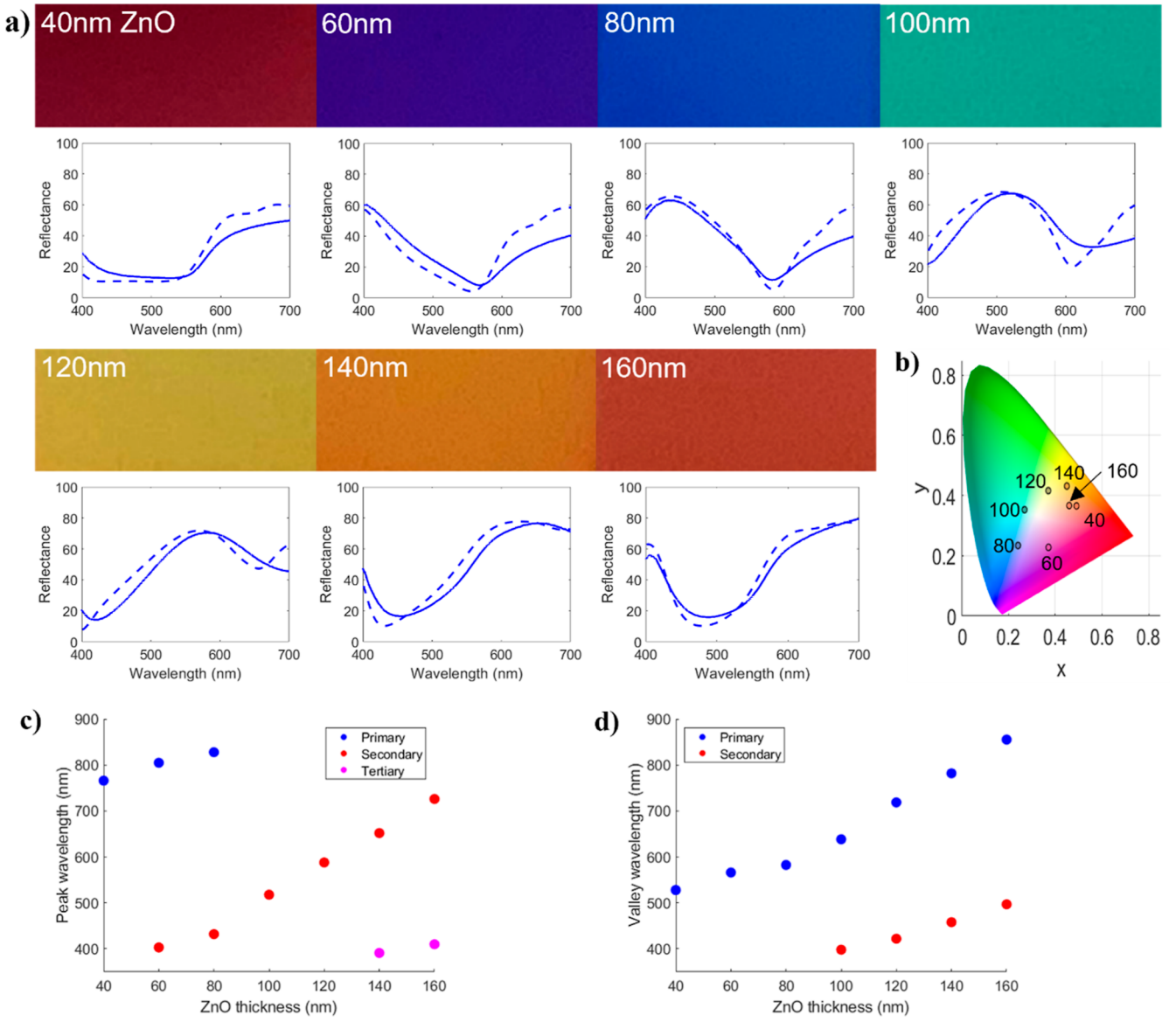

Figure 2. (a) Structural colors for planar MDM films with a range of ZnO thicknesses. Each color has a corresponding ZnO thickness listed. For each color, a digital photograph of the sample is provided, as well as both the measured and simulated optical reflectance spectra (solid line: measured; dashed line: simulated spectra). (b) RGB values of the simulated spectra shown in a chromaticity plot. At the bottom of the figure are plots of the primary and secondary (c) peaks and (d) valleys of the measured reflectance spectra as a function of dielectric thickness. These plots include data outside visible wavelengths.

RESULTS/DISCUSSION

To demonstrate the ability to tune structural colors using ALD, zinc oxide (ZnO) films were deposited with varying numbers of ALD cycles on a silicon substrate, with Ni metal as the bottom layer and Cu metal as the top layer. ZnO was selected as the dielectric layer, owing to its wide band gap (3.3 eV), relatively flat index of refraction (~2), and well-behaved ALD process. Cu was selected as the metal top layer because of its well-understood ALD process that can be easily tuned and because of its favorable optical absorption properties for MDM structures.[10] The base metal of these structures was a 50 nm thick nickel layer deposited by PVD atop a silicon substrate. In these planar samples, Ni was selected as the base metal as it is a highly reflective metal with broadband reflectance, although as we demonstrate later, this process is versatile and can produce structural color on a range of different substrates and base metal layers.

A cross-sectional scanning electron microscopy (SEM) image of a representative MDM structure fabricated by ALD is shown in Figure 1a, which is illustrated schematically in Figure 1b. This specific cavity had a dielectric thickness of 120 nm and a Cu top layer thickness of 20 nm, both of which can be tuned with sub-nanometer precision by varying the number of ALD cycles. The flat boundaries between layers show the uniform control of thickness and conformal interface between the various MDM layers, which are characteristics of ALD growth.

Figure 2 shows a range of colors possible with ALD MDM structures, which spans the full visible spectrum. The ZnO layer thickness was gradually increased from 40 to 160 nm, while the thickness of the top Cu layer was maintained at 20 nm. Each color, as shown in Figure 2a, has a respective measured and simulated reflectance spectrum. The simulations were performed using a transfer matrix method (TMM) to

https://doi.org/10.1021/acsami.2c05940
ACS Appl. Mater. Interfaces 2022, 14, 31099−31108

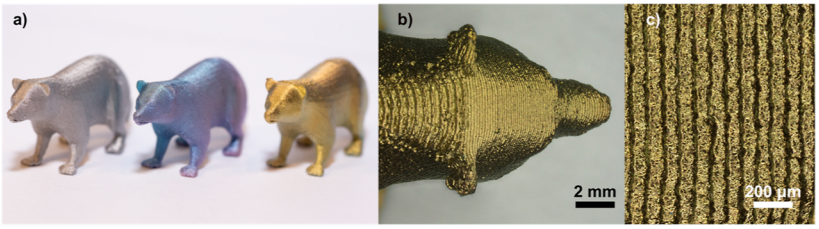

Figure 3. Imparting structural color onto metal 3D-printed objects with MDM coatings. (a) Wolverine figurines manufactured with metal 3D printing of stainless steel, including an uncoated control (left), coated with 80 nm of ZnO (center), and 120 nm of ZnO (right) as the dielectric layer. A 20 nm top layer of Cu was deposited for both ALD samples. (b,c) Optical microscopy images of the wolverine demonstrate conformal and uniform structural color, spanning the micro- to macroscales.

determine the optical reflectance spectra for a three-layer structure. To show the change in RGB values for this range of ZnO thicknesses, an International Commission on Illumination chromaticity plot is also included, as shown in Figure 2b.

Vivid colors can be observed from the optical photographs and experimental reflectance spectra of the MDM structures, as shown in Figure 2a. Previous work has shown that structural color can also be generated without a top metal layer, using only a dielectric layer atop a base metal (MD) or substrate (D).[51−53] Figure S2 shows the spectral advantages of the MDM structure over these architectures, where the addition of the top metal layer produces distinct peaks and valleys that are absent in the MD or D spectra. This effect is a result of copper being a good absorber of broadband visible light, which improves the color vibrancy.[10]

Figure 2 shows that a full color cycle can be realized by adjusting the dielectric layer thickness. With 40 nm thick ZnO, the sample exhibited a red color, at 80 nm a blue color, and the color shifted back to red around 160 nm. The simulated and measured spectra agree well for the range of dielectric thicknesses. Absorption resonances are observed at 566 nm for 60 nm thick film, 583 nm for 80 nm, 639 nm for 100 nm, and 719 nm for 120 nm thick films. Most of the spectral peaks exhibited a reflection magnitude of 70−80%, which is a large distinction when compared to the reflectance valleys at 10−20%. While the simulation deviates slightly from measurement in the red wavelengths for thicknesses up to 120 nm, the overall spectrum shape remains highly consistent with the measured spectra. These slight deviations may be attributed to surface roughness of the ALD copper top layer, which arises from its well-studied island nucleation and growth mode on oxide surfaces (further details are shown in Figure S3).[55,56]

The CIE plot in Figure 2b includes the RGB data from the simulated spectra, yielding a single revolution around the center as the dielectric thickness was increased from 40 to 160 nm. One feature to note is the close proximity of the points to the center, indicating that the MDM structural color films are quite bright. Owing to the sub-nanometer precision in dielectric thickness afforded by ALD, additional points along the entire visible spectrum shown in the CIE plot can be easily fabricated for a range of ZnO thicknesses from 40 to 160 nm. Larger dielectric thicknesses were not deposited for this study but will yield a similar cyclic color dependence on dielectric thickness.

The resonance peaks and valleys of the measured spectra from Figure 2a were recorded and are plotted in Figure 2c,d to study the mathematical relationship between color and dielectric thickness. The wavelength range of this figure extends beyond the visible wavelengths to provide additional data points. Figure 2c,d shows that the resonance peaks and valleys in the spectra depend linearly on the dielectric thickness. This demonstrates that the desired color can be precisely chosen based on peak and valley wavelength using the extrapolated linear relationship.

As the dielectric layer increases in thickness, the resonance peaks and valleys shift toward longer wavelengths. Eventually, these primary extrema extend beyond the wavelength range of the spectrometer, but new secondary extrema appear in the spectra at short wavelengths. For example, as shown in Figure 2, the peak at a wavelength of 500 nm (corresponding to a ZnO thickness of 100 nm) translated to a wavelength of 650 nm when the thickness of ZnO was increased to 140 and then shifted beyond the visible spectrum for thicker dielectric layers. The spectrum for the 160 nm thick ZnO film exhibited a secondary peak emerging from the left. For this range of thicknesses, primary, secondary, and tertiary resonance peaks were observed, while primary and secondary resonance valleys were observed. Overall, the MDM structures deposited with ALD showed a linear relationship between reflectance peaks/valleys and dielectric thickness, illustrating tunable control of structural color.

Imparting Structural Color on Metal 3D-Printed Objects. To demonstrate the power of ALD to impart structural color onto non-planar, complex topographies, MDM structures were deposited onto the surface of 3D-printed metal figurines of a wolverine, with an overall height of 15 mm (Figure 3). The printed metal was Ultrafuse 17-4 PH stainless steel, which served as the base metal layer for the MDM structure. To generate a blue color on the 3D-printed object surface, an 80 nm thick ZnO film was deposited. For the yellow color, a 120 nm thick ZnO was deposited. This is consistent with the results from Figure 2, which shows the versatility of the technique in order to "paint" structural color to different substrates.

After the dielectric layer deposition, a 20 nm Cu layer was also deposited with ALD. Vibrant blue and yellow colors were observed on the 3D-printed structures, where the surface color was uniform across all of the curved features of the part, as shown in Figure 3. As shown in Figure 3c, the ALD coating conformally coats into the microscopic porous surface topographies that are characteristic of metal 3D printing. This highlights the benefits of conformal gas-phase deposition to impart color to additively manufactured objects, covering surface topographies at length scales and aspect ratios that would be extremely challenging to coat with traditional paints.

To further quantify the conformality of the MDM structures, 600 ALD cycles of ZnO and 1000 ALD cycles of Cu were coated on etched Si trenches, as shown in Figure S4. 120 nm thick ZnO and 20 nm thick Cu can be observed along the full height of the trenches, including coating both convex and

https://doi.org/10.1021/acsami.2c05940
ACS Appl. Mater. Interfaces 2022, 14, 31099−31108

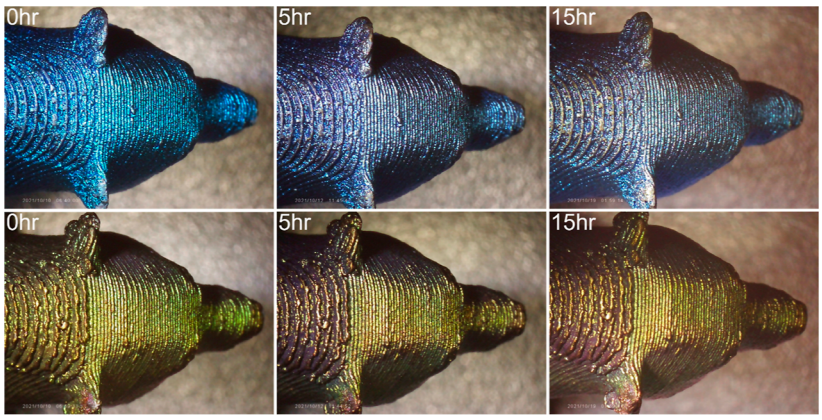

Figure 4. Thermal stability testing of blue and yellow wolverine figurines in ambient air at 300 °C. Both figurines had a protective alumina coat deposited with ALD, where the alumina thickness was selected such that it would behave as an anti-reflective layer.

Scheme 1. (a–f) Process Flow for Patterning Block "M" Structure with AS-ALD

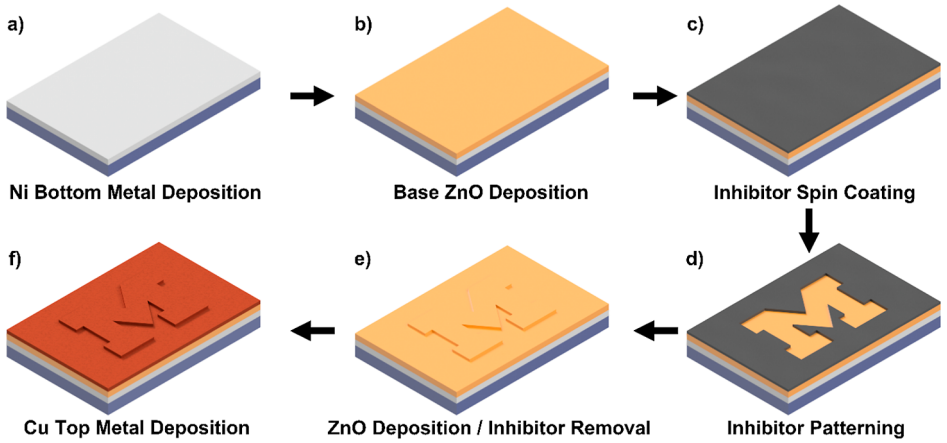

concave surface features. Additionally, a 40 mm diameter glass dome and a polyimide sheet were colored using a Fabry–Pérot cavity with 60 nm thick ZnO, as shown in Figure S5. Comparing the reflectance spectrum of the glass dome and polyimide respect to a planar Si substrate, all of the samples exhibited very similar absorption resonances at 566 nm. This demonstrates the powerful capability of ALD to impart structural color onto a wide range of high-aspect ratio, non-planar, and/or flexible substrates.

Improving Thermal Stability and Color Saturation with ALD Overcoats. One advantage of structural color layers over traditional polymer-based paints is their improved thermal stability, which arises from the use of entirely inorganic materials. While the constituent materials in this study may not surpass the best pigment-based paints, dielectric materials like Al_2O_3 are stable up to 800 °C.[57] Furthermore, with the proper choice of materials, the coating can also serve as a "shield" against thermochemical reactions such as oxidation in humid air. In our MDM structure, however, the top metal is copper which is prone to oxidation in ambient air, especially at elevated temperatures. Therefore, to improve the thermal stability of the structural color, we added an "overcoat" of Al_2O_3, which serves as a protective barrier for the Cu top metal layer, thereby forming a dielectric–metal–dielectric–metal structure.

In addition to the final Al_2O_3 overcoat acting as a protective layer, it also offers an interesting optical effect that can improve the color saturation significantly. When its thickness is chosen to be one-quarter of the resonance valley wavelength of the structure, it acts as an antireflection layer, ensuring near-perfect absorption of light in this wavelength range, while minimizing light absorption at a peak reflection wavelength.[58,59] The result is a more saturated color due to this protective top dielectric layer. To demonstrate this effect, the colored wolverine figurines in Figure 3 were coated with corresponding Al_2O_3 thickness: the blue figurine was coated with 91 nm, whereas the yellow was coated with 65 nm of Al_2O_3.

To test the thermal stability of the DMDM structures, the two coated wolverine figurines were baked at 300 °C for 5 h segments for a total of 15 h. The resulting surfaces are shown in optical microscopy images in Figure 4, including the as-deposited color, after a 5 h thermal treatment and after a 15 h thermal treatment. Both figurines retained their bright colors after 15 h of 300 °C baking without any evidence of peeling or delamination. Furthermore, planar stainless-steel substrates were coated to measure the reflectance spectra of analogous MDM and DMDM stacks under high-temperature conditions (Figure S6). These two studies demonstrate the ability to retain structural color on 3D-printed objects under conditions that would be incompatible with most polymeric paints. In the future, additional optimization of the overcoat can be performed using the wide range of available ALD chemistries and thicknesses under extreme conditions.

Area-Selective Patterning of Structural Color. In addition to complete coverage of the substrate, an additional benefit of using ALD to impart structural color is the

https://doi.org/10.1021/acsami.2c05940
ACS Appl. Mater. Interfaces 2022, 14, 31099–31108

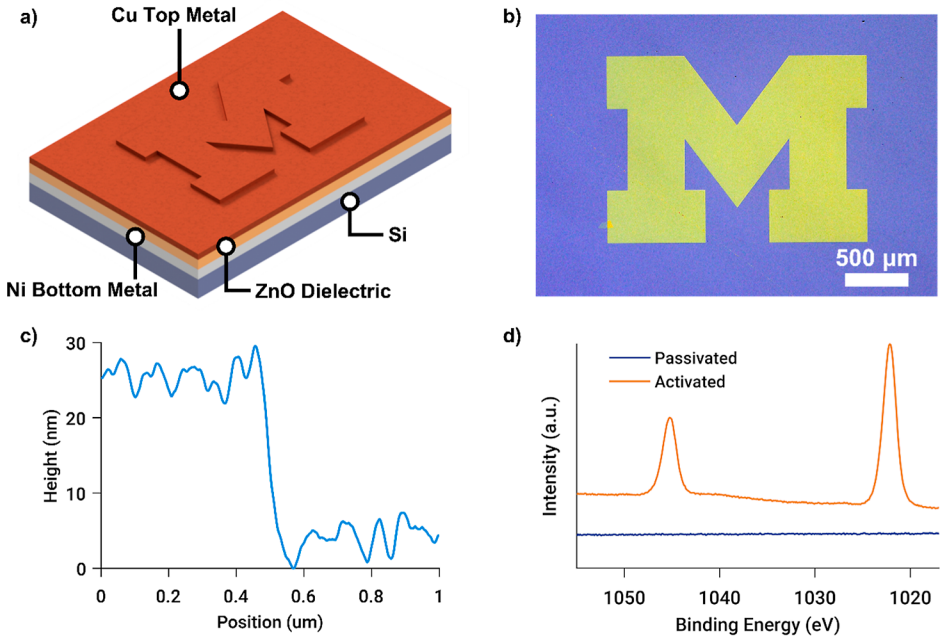

Figure 5. (a) Schematic of the MDM structure patterned by AS-ALD, where the ZnO layer within the M layer is thicker than the surrounding region, resulting in a color difference. (b) Optical microscopy image of the letter "M," where 90 nm of ZnO was deposited on the blue region and 120 nm of ZnO was deposited on the yellow region. (c) AFM image at the blue/yellow interface. (d) XPS core scans of the Zn 2p peak region on an inhibitor-coated (passivated) region and uncoated (activated) region.

possibility of selectively depositing colored patterns in prespecified regions. To demonstrate the feasibility of selective printing of structural colors using AS-ALD, a polymer inhibitor layer was patterned on the ZnO layer, as seen in Scheme 1. It has been previously shown that by selecting a polymer with surface functional groups that do not facilitate the necessary ligand-exchange reactions with the ALD precursor molecules, the nucleation and growth of ALD can be suppressed.[33,35,60−64] This facilitates a new strategy for integrating structural color with additively manufactured materials, as inhibiting polymers can be 3D-printed in specified regions, which will deactivate local ALD growth. By patterning the inhibitor and selectively depositing ZnO, the thickness of the films on different areas of the substrate can be tuned. This allows different structural colors to be patterned/painted on the same substrate where the thickness of ZnO would determine wavelength peaks and valleys.

To demonstrate the feasibility of AS-ALD of MDM structures, the letter "M" was patterned to generate a yellow core surrounded by a blue background. Ni metal was first evaporated on a Si substrate, and then, 90 nm of ZnO was deposited to provide the background blue color. Next, SPR 955 photoresist was spin-coated and patterned using photolithography to activate the "M" area by locally removing the polymer inhibitor layer. An extra 30 nm of ZnO was deposited to "paint" the activated zone with yellow. After removing the polymer inhibitor, the sample was coated with 20 nm of Cu ALD.

As a result, the patterned region exhibited the target colors of vibrant yellow and blue, as shown by the optical microscopy image in Figure 5b. X-ray photoelectron spectroscopy (XPS) analysis of the inhibited area on the substrate (Figure 5d) shows that ZnO deposition was completely inhibited as no visible Zn 2p peak was observed on the core scan. For the regions on the surface that did not have an inhibitor, the Zn 2p core spectra characteristic of ZnO growth were observed, with the expected stoichiometry.

To study the morphology of the selectively deposited films, atomic force microscopy (AFM) was performed across the border of the patterned "M" and the surrounding background region. A clear step edge can be observed, with a step height between the blue and yellow region that agrees well with the expected values of the ALD ZnO thickness based on spectroscopic ellipsometry measurements. Furthermore, the reflectance colors are consistent with the predicted values, where the dielectric thicknesses of the blue and yellow regions were approximately 90 and 120 nm, respectively. We note that this is not a traditional lift-off process, which would leave sidewalls along the boundary. Instead, by selecting a polymer that inhibits ALD growth, this is a purely additive process, where the ALD film only deposits locally in the unpatterned regions, resulting in a step edge. This demonstrates the feasibility of using AS-ALD to pattern structural colors, which we apply to an additive 3D-printing process in the following section.

Additive Nanomanufacturing of Structural Color with e-Jet Printing. While the pattern above was generated using photolithography, the approach of using printed polymers to pattern structural color is general, which opens up the possibility of integrating area-selective structural color with 3D-printing techniques. In particular, we have previously shown that electrohydrodynamic jet (e-jet) printing can be combined with AS-ALD to selectively deposit functional materials with sub-micrometer line widths (significantly below the resolution of ink-jet printing) while maintaining the sub-nanometer precision afforded by ALD in the *z*-direction.[44,45] We extend this approach here to demonstrate additive nanomanufacturing of structural colors.

To demonstrate structural-color printing using the combination of e-jet and AS-ALD, we printed polyvinylpyrrolidone

https://doi.org/10.1021/acsami.2c05940
ACS Appl. Mater. Interfaces 2022, 14, 31099−31108

(PVP) inks (5 wt % PVP dissolved in dimethyl sulfoxide) onto Si substrates to pattern specified thicknesses of ZnO with AS-ALD (Figure 5a). Prior to e-jet printing, a blanket film of ALD ZnO was first deposited to produce the desired font color, based on the color shown in Figure 2. To change the color of the surrounding background, a PVP inhibitor layer was e-jet printed on top of this blanket film, which preserved the ZnO thickness underneath. Subsequently, additional ALD ZnO cycles were performed to selectively change the surrounding (background) color as ZnO only grew on the unprinted surface regions (Figure 5a). As a result, the font color is determined by the blanket film thickness, and the surrounding background color can be precisely tuned by varying the thicknesses of ZnO that is deposited after e-jet printing.

As a proof of concept, an extra 40 nm of ZnO was deposited to change the background color for each printed font. Red, yellow, and blue texts were thereby generated by e-jet printing with a sub-10 μm resolution in line width. The printed text is illustrated in Figure 6 where different text and background

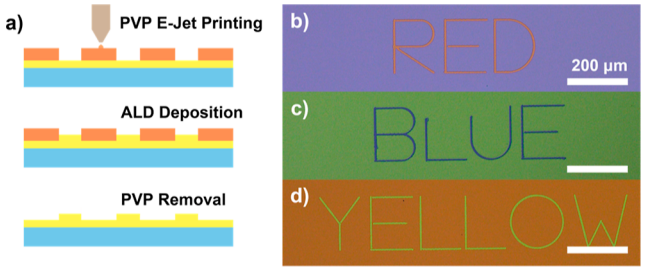

Figure 6. (a) Schematic showing the process flow for "structural color printing" using a combination of AS-ALD and e-jet [orange: polymer inhibitor (PVP), yellow: ALD ZnO, and blue: Si substrate]. (b–d) Optical microscopy images showing different colors with the text (red, blue, and yellow, respectively).

colors show the successful patterning of ZnO, with tunable control of both the font and background colors. This indicates that ZnO was selectively deposited on areas where PVP was not printed.

The combination of e-jet printing with AS-ALD enables a route to high-resolution additive manufacturing with structural color by providing a precise control over the ejection, volume, and depositing position of ink droplets onto a substrate.[44] Furthermore, while a planar substrate was used for simplicity here, e-jet is a versatile technique that also print on top of non-planar and flexible substates.[65,66] This opens up the possibility of integrating additive nanomanufacturing with structural color into even more complex 3D geometries in the future, including hierarchical architectures that span nano- to macro-length scales.

CONCLUSIONS

In this work, we demonstrated the use of ALD to fabricate MDM Fabry–Pérot cavities with bright and tunable structural color palettes that span the visible spectrum and are stable in high-temperature conditions. To demonstrate the potential of ALD to integrate structural color with additive manufacturing, we apply this technique to impart color onto both macroscopic 3D-printed metal objects, as well as microscale patterns generated by e-jet printing. In addition to blanket coverage of 3D-printed objects, we show that by printing inhibitor layers, structural colors can be selectively patterned in pre-specified areas through AS-ALD. Color printing with nanoscale precision is feasible with this method since e-jet can print down to sub-100 nm features, and ALD facilitates the control of the dielectric thickness with sub-nanometer precision.

We should point out that the MDM structure used in this work is only a representative structure, primarily for its simplicity that only uses ZnO and Cu as a proof-of-concept material system. This pair cannot satisfy high-temperature requirements, especially Cu. Structural colors can be designed purely with dielectric materials though, as shown in our previous work.[6,13,67] They can also be designed with a dielectric layer overcoat to protect the thin metal layer.[68] In fact, structural colors can utilize a variety of structures and materials,[10] and machine learning can assist with the design automatically when a list of materials are provided.[69,70] Such a list can include criteria like thermal expansion matching and high-temperature stability.

In the future, we envision that the integration of structural color with 3D-printing processes can open up new avenues for additive manufacturing, where aesthetics and optical properties are critical. In particular, the ability to conformally coat high-aspect-ratio non-planar surfaces, including those with re-entrant geometries, would be very difficult to accomplish with traditional paints without sacrificing geometric specificity. Furthermore, ALD can deposit a wide range of materials in the periodic table, including oxides, nitrides, sulfides, and metallic films.[19,36,71−76] This provides a versatile "toolbox" for additive manufacturing with structural color, with potential applications in optics, photovoltaics, circuits, and far more.

METHODS

Electron Beam Evaporation. For the planar samples, the base metal layer for each sample was deposited onto silicon using evaporation in an Angstrom Engineering Evovac Evaporator. The evaporated film thickness was 50 nm with a deposition rate of 3 Å/s.

Atomic Layer Deposition. A custom-built, hot wall, cross flow thermal ALD reactor was used to deposit zinc-oxide (ZnO) on the substrates. The precursors used were diethylzinc (DEZ, Sigma-Aldrich, St. Louis, MO, ≥52 wt % Zn basis) as the metalorganic precursor and deionized water (DI water) as the oxidant. Both precursors were kept at room temperature. The deposition temperature was 130 °C where argon (Ar) was used as the carrier gas at 70 sccm. For the ZnO deposition cycle, DEZ was pulsed for 0.05 s, then it was purged for 30 s, DI water was pulsed for 0.1 s, then it was purged for 30 s. This was repeated until the desired ZnO thickness is obtained. The average growth rate on silicon wafer piece was measured to be 2 Å/cycle.

For copper (Cu) ALD deposition, a Veeco Fiji G2 flow-type ALD tool was used with $[Cu(^{s}Bu\text{-}amd)]_2$ for the Cu precursor and hydrogen plasma at 300 W. The source temperature was kept at 110 °C with bubbler setup. The Cu ALD films were deposited at 185 °C where Ar was used as the carrier gas at 110 sccm. Each Cu ALD cycle was 3 s pulse of Cu precursor, 8 s purge, 300 W hydrogen plasma exposure for 10 s, and purged for 8 s. The average growth rate was measured to be 0.2 Å/cycle.

Material Characterization. Spectroscopic ellipsometry was performed with a J. A. Woollam M-2000 ellipsometer using a Cauchy model (wavelength range: 400–1600 nm, three angles of incidence: 65°, 70°, and 75°) to measure the thickness of ALD films. XPS was performed using a Kratos Axis Ultra XPS, with a monochromatic Al source (10 mA, 12 kV) with a pass energy 20 eV and a step size of 0.1 eV on a spot size of 700 μm by 300 μm. The obtained XPS spectra were analyzed using CasaXPS software. SEM images were taken using FEI Helios 650 Nanolab SEM at 2 kV and 100 pA. AFM was performed with a MFP-3D Origin+ AFM from Asylum Research. Reflectance spectra at normal incidence were measured using a thin-

https://doi.org/10.1021/acsami.2c05940
ACS Appl. Mater. Interfaces 2022, 14, 31099−31108

film measurement spectrometer (Ocean Optics Inc. HR4000CG-UV-NIR High-Resolution Spectrometer) integrated with a white light source.

Inhibitor Patterning and AS-ALD. E-jet printing experiments are conducted using a custom-built e-jet printer setup at the University of Michigan with an integrated Nanosurf Nanite AFM. The setup includes an $X-Y-Z$ nanopositioning stage, a voltage amplifier, a function generator, a camera, and a light source for nozzle alignment and jetting visualization with 10× magnification lensing, and a nozzle mount to hold the micropipette nozzles. 5 wt % PVP in DMSO was used as the ink material, which is filtered with a 0.22 μm pore size filter to avoid nozzle clogging. 2 μm opening micropipette nozzles were provided from World Precision Instruments (WPI) with an offset of 20 μm from the substrate. Pulse printing is used for printing the patterns with a high voltage of 370 V, a low voltage of 255 V, and a pulse duration of 90 μs. The voltage frequency and the stage speed during printing the patterns were 100 Hz and 1 mm/s, respectively.

Inhibitor-patterned substrates were then transferred to the ALD chamber for AS-ALD of ZnO. After ALD deposition, the substrates were sonicated in acetone and isopropanol for 10 min to remove the inhibitor polymer.

Reflectance Simulation. The simulated reflectance spectra were calculated using a TMM approach in MATLAB. Optical constant data for the ZnO and copper layers were measured with ellipsometry, described in the Material Characterization section. Nickel optical constant data were obtained from an online database (Johnson and Christy, 1974). The bottom silicon layer was treated as an infinite domain to ensure no light transmission. The imaginary optical constant of ZnO was set to zero to achieve a better fit.

■ ASSOCIATED CONTENT

Supporting Information

The Supporting Information is available free of charge at https://pubs.acs.org/doi/10.1021/acsami.2c05940.

> Reflectance spectrum of different metal/dielectric layers, SEM image of ALD ZnO and Cu on Si and Si trenches, and reflectance spectrum of the MDM structure on different substrates (glass dome, polyimide, and planar Si) (PDF)

■ AUTHOR INFORMATION

Corresponding Authors

Kira Barton − *Department of Mechanical Engineering, University of Michigan, Ann Arbor, Michigan 48109, United States*; Email: bartonkl@umich.edu

Neil P. Dasgupta − *Department of Mechanical Engineering and Department of Materials Science & Engineering, University of Michigan, Ann Arbor, Michigan 48109, United States*; orcid.org/0000-0002-5180-4063; Email: ndasgupt@umich.edu

L. Jay Guo − *Deparment of Applied Physics, University of Michigan, Ann Arbor, Michigan 48109, United States; Department of Mechanical Engineering and Department of Electrical Engineering and Computer Science, University of Michigan, Ann Arbor, Michigan 48109, United States;* orcid.org/0000-0002-0347-6309; Email: guo@umich.edu

Authors

Benjamin A. Rorem − *Deparment of Applied Physics, University of Michigan, Ann Arbor, Michigan 48109, United States;* orcid.org/0000-0003-0190-5090

Tae H. Cho − *Department of Mechanical Engineering, University of Michigan, Ann Arbor, Michigan 48109, United States*

Nazanin Farjam − *Department of Mechanical Engineering, University of Michigan, Ann Arbor, Michigan 48109, United States*

Julia D. Lenef − *Department of Materials Science & Engineering, University of Michigan, Ann Arbor, Michigan 48109, United States*

Complete contact information is available at: https://pubs.acs.org/10.1021/acsami.2c05940

Author Contributions

⊥B.A.R. and T.H.C. contributed equally to this work.

Notes

The authors declare no competing financial interest.

■ ACKNOWLEDGMENTS

This material is based upon work supported by the National Science Foundation under grant nos. 1727918 and 1751590. Portions of this work were performed at the Lurie Nanofabrication Facility and the Michigan Center for Materials Characterization, which are supported by the College of Engineering at University of Michigan.

■ REFERENCES

(1) Arsenault, A. C.; Puzzo, D. P.; Manners, I.; Ozin, G. A. Photonic-Crystal Full-Colour Displays. *Nat. Photonics* **2007**, *1*, 468−472.

(2) Hong, J.; Chan, E.; Chang, T.; Fung, T.-C.; Hong, B.; Kim, C.; Ma, J.; Pan, Y.; Lier, R. V.; Wang, S.-g.; Wen, B.; Zhou, L. Continuous Color Reflective Displays Using Interferometric Absorption. *Optica* **2015**, *2*, 589.

(3) Zhu, X.; Vannahme, C.; Højlund-Nielsen, E.; Mortensen, N. A.; Kristensen, A. Plasmonic Colour Laser Printing. *Nat. Nanotechnol.* **2016**, *11*, 325−329.

(4) Kumar, K.; Duan, H.; Hegde, R. S.; Koh, S. C. W.; Wei, J. N.; Yang, J. K. W. Printing Colour at the Optical Diffraction Limit. *Nat. Nanotechnol.* **2012**, *7*, 557−561.

(5) Kim, H.; Ge, J.; Kim, J.; Choi, S.-e.; Lee, H.; Lee, H.; Park, W.; Yin, Y.; Kwon, S. Structural Colour Printing Using a Magnetically Tunable and Lithographically Fixable Photonic Crystal. *Nat. Photonics* **2009**, *3*, 534−540.

(6) Lee, K.-T.; Ji, C.; Banerjee, D.; Guo, L. J. Angular- and Polarization-Independent Structural Colors Based on 1D Photonic Crystals. *Laser Photonics Rev.* **2015**, *9*, 354−362.

(7) Banerjee, D.; Zhang, M. Quarter-Wave Design Criteria for Omnidirectional Structural Colors. *J. Mod. Opt.* **2010**, *57*, 1180−1188.

(8) Masuda, T.; Kudo, Y.; Banerjee, D. Visually Attractive and High-Power-Retention Solar Modules by Coloring with Automotive Paints. *Coatings* **2018**, *8*, 282.

(9) Masuda, T.; Hirai, S.; Inoue, M.; Chantana, J.; Kudo, Y.; Minemoto, T. Colorful, Flexible, and Lightweight Cu(In,Ga)Se2 Solar Cell by Lift-Off Process with Automotive Painting. *IEEE J. Photovoltaics* **2018**, *8*, 1326−1330.

(10) Ji, C.; Lee, K. T.; Xu, T.; Zhou, J.; Park, H. J.; Guo, L. J. Engineering Light at the Nanoscale: Structural Color Filters and Broadband Perfect Absorbers. *Advanced Optical Materials*; Wiley-VCH Verlag, 2017; Vol. *16*.

(11) Xu, G.; Shen, L.; Cui, C.; Wen, S.; Xue, R.; Chen, W.; Chen, H.; Zhang, J.; Li, H.; Li, Y.; Li, Y. High-Performance Colorful Semitransparent Polymer Solar Cells with Ultrathin Hybrid-Metal Electrodes and Fine-Tuned Dielectric Mirrors. *Adv. Funct. Mater.* **2017**, *27*, 1605908.

(12) Lu, J.-H.; Lin, Y. H.; Jiang, B. H.; Yeh, C. H.; Kao, J. C.; Chen, C. P. Microcavity Structure Provides High-Performance (>8.1%)

Semitransparent and Colorful Organic Photovoltaics. *Adv. Funct. Mater.* **2018**, *28*, 1703398.
(13) Ji, C.; Zhang, Z.; Masuda, T.; Kudo, Y.; Guo, L. J. Vivid-Colored Silicon Solar Panels with High Efficiency and Non-Iridescent Appearance. *Nanoscale Horiz.* **2019**, *4*, 874−880.
(14) Sabnis, R. W. Color Filter Technology for Liquid Crystal Displays. *Displays* **1999**, *20*, 119.
(15) Li, Z.; Butun, S.; Aydin, K. Large-Area, Lithography-Free Super Absorbers and Color Filters at Visible Frequencies Using Ultrathin Metallic Films. *ACS Photonics* **2015**, *2*, 183−188.
(16) Yang, C.; Shen, W.; Zhang, Y.; Li, K.; Fang, X.; Zhang, X.; Liu, X. Compact Multilayer Film Structure for Angle Insensitive Color Filtering. *Sci. Rep.* **2015**, *5*, 9285.
(17) Ji, C.; Acharya, S.; Yamada, K.; Maldonado, S.; Guo, L. J. Electrodeposition of Large Area, Angle-Insensitive Multilayered Structural Colors. *ACS Appl. Mater. Interfaces* **2019**, *11*, 29065−29071.
(18) Dasgupta, N. P.; Lee, H.-B. -R.; Bent, S. F.; Weiss, P. S. Recent Advances in Atomic Layer Deposition. *Chem. Mater.* **2016**, *28*, 1943−1947.
(19) George, S. M. Atomic Layer Deposition: An Overview. *Chem. Rev.* **2010**, *110*, 111−131.
(20) Gayle, A. J.; Berquist, Z. J.; Chen, Y.; Hill, A. J.; Hoffman, J. Y.; Bielinski, A. R.; Lenert, A.; Dasgupta, N. P. Tunable Atomic Layer Deposition into Ultra-High-Aspect-Ratio (>60000:1) Aerogel Monoliths Enabled by Transport Modeling. *Chem. Mater.* **2021**, *33*, 5572−5583.
(21) Rodríguez, R. E.; Agarwal, S. P.; An, S.; Kazyak, E.; Das, D.; Shang, W.; Skye, R.; Deng, T.; Dasgupta, N. P. Biotemplated Morpho Butterfly Wings for Tunable Structurally Colored Photocatalysts. *ACS Appl. Mater. Interfaces* **2018**, *10*, 4614−4621.
(22) Bielinski, A. R.; Boban, M.; He, Y.; Kazyak, E.; Lee, D. H.; Wang, C.; Tuteja, A.; Dasgupta, N. P. Rational Design of Hyperbranched Nanowire Systems for Tunable Superomniphobic Surfaces Enabled by Atomic Layer Deposition. *ACS Nano* **2017**, *11*, 478−489.
(23) Kazyak, E.; Chen, K. H.; Chen, Y.; Cho, T. H.; Dasgupta, N. P. Enabling 4C Fast Charging of Lithium-Ion Batteries by Coating Graphite with a Solid-State Electrolyte. *Adv. Energy Mater.* **2022**, *12*, 2102618.
(24) Cremers, V.; Puurunen, R. L.; Dendooven, J. Conformality in Atomic Layer Deposition: Current Status Overview of Analysis and Modelling. *Appl. Phys. Rev.* **2019**, *6*, 021302.
(25) Knez, M.; Nielsch, K.; Niinistö, L. Synthesis and Surface Engineering of Complex Nanostructures by Atomic Layer Deposition. *Adv. Mater.* **2007**, *19*, 3425−3438.
(26) Chen, Y.; Ginga, N. J.; LePage, W. S.; Kazyak, E.; Gayle, A. J.; Wang, J.; Rodríguez, R. E.; Thouless, M. D.; Dasgupta, N. P. Enhanced Interfacial Toughness of Thermoplastic-Epoxy Interfaces Using ALD Surface Treatments. *ACS Appl. Mater. Interfaces* **2019**, *11*, 43573−43580.
(27) Bielinski, A. R.; Kazyak, E.; Schlepütz, C. M.; Jung, H. J.; Wood, K. N.; Dasgupta, N. P. Hierarchical ZnO Nanowire Growth with Tunable Orientations on Versatile Substrates Using Atomic Layer Deposition Seeding. *Chem. Mater.* **2015**, *27*, 4799−4807.
(28) Ellinger, C. R.; Nelson, S. F. Selective Area Spatial Atomic Layer Deposition of ZnO, Al 2 O 3 , and Aluminum-Doped ZnO Using Poly(Vinyl Pyrrolidone). *Chem. Mater.* **2014**, *24*, 1514.
(29) Poodt, P.; Kniknie, B.; Branca, A.; Winands, H.; Roozeboom, F. Patterned Deposition by Plasma Enhanced Spatial Atomic Layer Deposition. *Phys. Status Solidi RRL* **2011**, *5*, 165−167.
(30) Katsouras, I.; Frijters, C.; Poodt, P.; Gelinck, G.; Kronemeijer, A. J. Large-area Spatial Atomic Layer Deposition of Amorphous Oxide Semiconductors at Atmospheric Pressure. *J. Soc. Inf. Disp.* **2019**, *27*, 304.
(31) Ng, S.; Iffelsberger, C.; Michalička, J.; Pumera, M. Atomic Layer Deposition of Electrocatalytic Insulator Al2O3on Three-Dimensional Printed Nanocarbons. *ACS Nano* **2021**, *15*, 686−697.
(32) Ng, S.; Zazpe, R.; Rodriguez-Pereira, J.; Michalička, J.; Macak, J. M.; Pumera, M. Atomic Layer Deposition of Photoelectrocatalytic Material on 3D-Printed Nanocarbon Structures. *J. Mater. Chem. A* **2021**, *9*, 11405−11414.
(33) Parsons, G. N.; Clark, R. D. Area-Selective Deposition: Fundamentals, Applications, and Future Outlook. *Chem. Mater.* **2020**, *32*, 4920−4953.
(34) Lee, H.-B. -R.; Bent, S. F. A Selective Toolbox for Nanofabrication. *Chem. Mater.* **2020**, *32*, 3323−3324.
(35) Mackus, A. J. M.; Merkx, M. J. M.; Kessels, W. M. M. From the Bottom-Up : Toward Area-Selective Atomic Layer Deposition with High Selectivity †. *Chem. Mater.* **2019**, *31*, 2.
(36) Lee, W.; Dasgupta, N. P.; Trejo, O.; Lee, J.-R.; Hwang, J.; Usui, T.; Prinz, F. B. Area-Selective Atomic Layer Deposition of Lead Sulfide : Nanoscale Patterning and DFT Simulations. *Langmuir* **2010**, *26*, 6845−6852.
(37) Bobb-Semple, D.; Nardi, K. L.; Draeger, N.; Hausmann, D. M.; Bent, S. F. Area-Selective Atomic Layer Deposition Assisted by Self-Assembled Monolayers: A Comparison of Cu, Co, W, and Ru. *Chem. Mater.* **2019**, *31*, 1635−1645.
(38) MacKus, A. J. M.; Dielissen, S. A. F.; Mulders, J. J. L.; Kessels, W. M. M. Nanopatterning by Direct-Write Atomic Layer Deposition. *Nanoscale* **2012**, *4*, 4477−4480.
(39) Levy, D. H.; Ellinger, C. R.; Nelson, S. F. Metal-Oxide Thin-Film Transistors Patterned by Printing. *Appl. Phys. Lett.* **2013**, *103*, 043505.
(40) Sinha, A.; Hess, D. W.; Henderson, C. L. Area Selective Atomic Layer Deposition of Titanium Dioxide: Effect of Precursor Chemistry. *J. Vac. Sci. Technol., B: Microelectron. Nanometer Struct.–Process., Meas., Phenom.* **2006**, *24*, 2523.
(41) Jiang, X.; Bent, S. F. Area-Selective ALD with Soft Lithographic Methods: Using Self-Assembled Monolayers to Direct Film Deposition. *J. Phys. Chem. C* **2009**, *113*, 17613−17625.
(42) Mameli, A.; Karasulu, B.; Verheijen, M. A.; Barcones, B.; Macco, B.; Mackus, A. J. M.; Kessels, W. M. M. E.; Roozeboom, F. Area-Selective Atomic Layer Deposition of ZnO by Area Activation Using Electron Beam-Induced Deposition. *Chem. Mater.* **2019**, *31*, 1250−1257.
(43) Ellinger, C. R.; Nelson, S. F. Selective Area Spatial Atomic Layer Deposition of ZnO, Al2O 3, and Aluminum-Doped ZnO Using Poly(Vinyl Pyrrolidone). *Chem. Mater.* **2014**, *26*, 1514−1522.
(44) Cho, T. H.; Farjam, N.; Allemang, C. R.; Pannier, C. P.; Kazyak, E.; Huber, C.; Rose, M.; Trejo, O.; Peterson, R. L.; Barton, K.; Dasgupta, N. P. Area-Selective Atomic Layer Deposition Patterned by Electrohydrodynamic Jet Printing for Additive Manufacturing of Functional Materials and Devices. *ACS Nano* **2020**, *14*, 17262−17272.
(45) Farjam, N.; Cho, T. H.; Dasgupta, N. P.; Barton, K. Subtractive Patterning: High-Resolution Electrohydrodynamic Jet Printing with Solvents. *Appl. Phys. Lett.* **2020**, *117*, 133702.
(46) Li, K.; Li, T.; Zhang, T.; Li, H.; Li, A.; Li, Z.; Lai, X.; Hou, X.; Wang, Y.; Shi, L.; Li, M.; Song, Y. Facile Full-Color Printing with a Single Transparent Ink. *Sci. Adv.* **2021**, *7*, No. eabh1992.
(47) Engstrom, D. S.; Porter, B.; Pacios, M.; Bhaskaran, H. Additive Nanomanufacturing - A Review. *J. Mater. Res.* **2014**, *29*, 1792−1816.
(48) Park, J.-U.; Hardy, M.; Kang, S. J.; Barton, K.; Adair, K.; Mukhopadhyay, D. K.; Lee, C. Y.; Strano, M. S.; Alleyne, A. G.; Georgiadis, J. G.; Ferreira, P. M.; Rogers, J. A. High-Resolution Electrohydrodynamic Jet Printing. *Nat. Mater.* **2007**, *6*, 782−789.
(49) Onses, M. S.; Sutanto, E.; Ferreira, P. M.; Alleyne, A. G.; Rogers, J. A. Mechanisms, Capabilities, and Applications of High-Resolution Electrohydrodynamic Jet Printing. *Small* **2015**, *11*, 4237−4266.
(50) Miikkulainen, V.; Leskelä, M.; Ritala, M.; Puurunen, R. L. Crystallinity of Inorganic Films Grown by Atomic Layer Deposition: Overview and General Trends. *J. Appl. Phys.* **2013**, *113*, 021301.
(51) Greenstein, L. M. *Pigment Handbook: Properties and Economics*; Patton, T. C., Ed.; John Wiley and Sons: New York, 1973; Vol. *1*, 871−890.

https://doi.org/10.1021/acsami.2c05940
ACS Appl. Mater. Interfaces 2022, 14, 31099−31108

(52) Kats, M. A.; Blanchard, R.; Genevet, P.; Capasso, F. Nanometre Optical Coatings Based on Strong Interference Effects in Highly Absorbing Media. *Nat. Mater.* **2013**, *12*, 20−24.
(53) Kats, M. A.; Byrnes, S. J.; Blanchard, R.; Kolle, M.; Genevet, P.; Aizenberg, J.; Capasso, F. Enhancement of Absorption and Color Contrast in Ultra-Thin Highly Absorbing Optical Coatings. *Appl. Phys. Lett.* **2013**, *103*, 101104.
(54) de Kersauson, M.; Kurdi, M. E.; David, S.; Checoury, X.; Fishman, G.; Sauvage, S.; Jakomin, R.; Beaudoin, G.; Sagnes, I.; Boucaud, P. Optical Gain in Single Tensile-Strained Germanium Photonic Wire. *Opt. Express* **2011**, *19*, 17925.
(55) Lenef, J. D.; Jo, J.; Trejo, O.; Mandia, D. J.; Peterson, R. L.; Dasgupta, N. P. Plasma-Enhanced Atomic Layer Deposition of p-Type Copper Oxide Semiconductors with Tunable Phase, Oxidation State, and Morphology. *J. Phys. Chem. C* **2021**, *125*, 9383−9390.
(56) Li, Z.; Rahtu, A.; Gordon, R. G. Atomic Layer Deposition of Ultrathin Copper Metal Films from a Liquid Copper(I) Amidinate Precursor. *J. Electrochem. Soc.* **2006**, *153*, C787.
(57) Berquist, Z. J.; Gayle, A. J.; Dasgupta, N. P.; Lenert, A. Transparent Refractory Aerogels for Efficient Spectral Control in High-Temperature Solar Power Generation. *Adv. Funct. Mater.* **2022**, *32*, 2108774.
(58) Yang, Z.; Ji, C.; Cui, Q.; Guo, L. J. High-Purity Hybrid Structural Colors by Enhancing Optical Absorption of Organic Dyes in Resonant Cavity. *Adv. Opt. Mater.* **2020**, *8*, 2000317.
(59) Yang, Z.; Ji, C.; Liu, D.; Guo, L. J. Enhancing the Purity of Reflective Structural Colors with Ultrathin Bilayer Media as Effective Ideal Absorbers. *Adv. Opt. Mater.* **2019**, *7*, 1900739.
(60) Färm, E.; Kemell, M.; Santala, E.; Ritala, M.; Leskelä, M. Selective-Area Atomic Layer Deposition Using Poly(Vinyl Pyrrolidone) as a Passivation Layer. *J. Electrochem. Soc.* **2010**, *157*, K10.
(61) Färm, E.; Kemell, M.; Ritala, M.; Leskelä, M. Selective-Area Atomic Layer Deposition Using Poly(Methyl Methacrylate) Films as Mask Layers. *J. Phys. Chem. C* **2008**, *112*, 15791−15795.
(62) Richey, N. E.; De Paula, C.; Bent, S. F. Understanding Chemical and Physical Mechanisms in Atomic Layer Deposition. *J. Chem. Phys.* **2020**, *152*, 040902.
(63) Lee, H.-B. -R. The Era of Atomic Crafting. *Chem. Mater.* **2019**, *31*, 1471−1472.
(64) Mackus, A. J. M.; Bol, A. A.; Kessels, W. M. M. The Use of Atomic Layer Deposition in Advanced Nanopatterning. *Nanoscale* **2014**, *6*, 10941−10960.
(65) Tse, L.; Barton, K. A Field Shaping Printhead for High-Resolution Electrohydrodynamic Jet Printing onto Non-Conductive and Uneven Surfaces. *Appl. Phys. Lett.* **2014**, *104*, 143510.
(66) Tse, L.; Barton, K. Airflow Assisted Printhead for High-Resolution Electrohydrodynamic Jet Printing onto Non-Conductive and Tilted Surfaces. *Appl. Phys. Lett.* **2015**, *107*, 054103.
(67) Ji, C.; Yang, C.; Shen, W.; Lee, K.-T.; Zhang, Y.; Liu, X.; Guo, L. J. Decorative Near-Infrared Transmission Filters Featuring High-Efficiency and Angular-Insensitivity Employing 1D Photonic Crystals. *Nano Res.* **2019**, *12*, 543−548.
(68) Ji, C.; Lee, K.-T.; Guo, L. J. High-Color-Purity, Angle-Invariant, and Bidirectional Structural Colors Based on Higher-Order Resonances. *Opt. Lett.* **2019**, *44*, 86.
(69) Wang, H.; Guo, L. J. NEUTRON: Neural Particle Swarm Optimization for Material-Aware Inverse Design of Structural Color. *iScience* **2022**, *25*, 104339.
(70) Wang, H.; Zheng, Z.; Ji, C.; Jay Guo, L. Automated Multi-Layer Optical Design via Deep Reinforcement Learning. *Mach. Learn.* **2021**, *2*, 025013.
(71) Kazyak, E.; Chen, K.-H.; Wood, K. N.; Davis, A. L.; Thompson, T.; Bielinski, A. R.; Sanchez, A. J.; Wang, X.; Wang, C.; Sakamoto, J.; Dasgupta, N. P. Atomic Layer Deposition of the Solid Electrolyte Garnet Li7La3Zr2O12. *Chem. Mater.* **2017**, *29*, 3785−3792.
(72) Mackus, A. J. M.; Schneider, J. R.; Macisaac, C.; Baker, J. G.; Bent, S. F. Synthesis of Doped, Ternary, and Quaternary Materials by Atomic Layer Deposition: A Review. *Chem. Mater.* **2019**, *31*, 1142−1183.
(73) Dasgupta, N. P.; Neubert, S.; Lee, W.; Trejo, O.; Lee, J.-R.; Prinz, F. B. Atomic Layer Deposition of Al-Doped ZnO Films: Effect of Grain Orientation on Conductivity. *Chem. Mater.* **2010**, *22*, 4769−4775.
(74) Bielinski, A. R.; Lee, S.; Brancho, J. J.; Esarey, S. L.; Gayle, A. J.; Kazyak, E.; Sun, K.; Bartlett, B. M.; Dasgupta, N. P. Atomic Layer Deposition of Bismuth Vanadate Core-Shell Nanowire Photoanodes. *Chem. Mater.* **2019**, *31*, 3221−3227.
(75) Allemang, C. R.; Cho, T. H.; Trejo, O.; Ravan, S.; Rodríguez, R. E.; Dasgupta, N. P.; Peterson, R. L. High-Performance Zinc Tin Oxide TFTs with Active Layers Deposited by Atomic Layer Deposition. *Adv. Electron. Mater.* **2020**, *6*, 2000195.
(76) Ande, C. K.; Knoops, H. C. M.; De Peuter, K.; Van Drunen, M.; Elliott, S. D.; Kessels, W. M. M. Role of Surface Termination in Atomic Layer Deposition of Silicon Nitride. *J. Phys. Chem. Lett.* **2015**, *6*, 3610−3614.

https://doi.org/10.1021/acsami.2c05940
ACS Appl. Mater. Interfaces 2022, 14, 31099−31108